



# **An improved setup for radial diffraction experiments at high pressures and high temperatures in a resistive graphite-heated diamond anvil cell**

Julia Immoor, Hauke Marquardt, Lowell M Miyagi, S. Speziale, Sébastien Merkel, I. Schwark, A. Ehnes, Hanns-Peter Liermann

## **► To cite this version:**

Julia Immoor, Hauke Marquardt, Lowell M Miyagi, S. Speziale, Sébastien Merkel, et al.. An improved setup for radial diffraction experiments at high pressures and high temperatures in a resistive graphite-heated diamond anvil cell. Review of Scientific Instruments, 2020, Review of Scientific Instruments, 91 (4), pp.045121. 10.1063/1.5143293 . hal-02558603

**HAL Id: hal-02558603**

**<https://hal.univ-lille.fr/hal-02558603>**

Submitted on 29 Apr 2020

**HAL** is a multi-disciplinary open access archive for the deposit and dissemination of scientific research documents, whether they are published or not. The documents may come from teaching and research institutions in France or abroad, or from public or private research centers.

L'archive ouverte pluridisciplinaire **HAL**, est destinée au dépôt et à la diffusion de documents scientifiques de niveau recherche, publiés ou non, émanant des établissements d'enseignement et de recherche français ou étrangers, des laboratoires publics ou privés.

1 An improved setup for radial diffraction experiments at high  
2 pressures and high temperatures in a resistive graphite-heated  
3 diamond anvil cell.

4 J. Immoor<sup>1</sup>, H. Marquardt<sup>2</sup>, L. Miyagi<sup>3</sup>, S. Speziale<sup>4</sup>, S. Merkel<sup>5</sup>, I. Schwark<sup>6</sup>, A. Ehnes<sup>6</sup>, H.-  
5 P. Liermann<sup>6</sup>

6 <sup>1</sup>Bayerisches Geoinstitut BGI, University of Bayreuth, 95440 Bayreuth, Germany;

7 <sup>2</sup>Department of Earth Sciences, University of Oxford, Oxford OX1 3AN, UK; <sup>3</sup>University of

8 Utah, 115 So. 1460 E., Salt Lake City, UT84112-0111, USA; <sup>4</sup>German Research Center for

9 Geosciences GFZ, 14473 Potsdam, Germany; <sup>5</sup>Univ. Lille, CNRS, INRAE, Centrale Lille,

10 UMR 8207 - UMET - Unité Matériaux et Transformations, F-59000 Lille, France; <sup>6</sup>Photon

11 Sciences, Deutsches Elektronen-Synchrotron (DESY), 22607 Hamburg, Germany

12 \*Correspondence to: Julia.immoor@uni-bayreuth.de

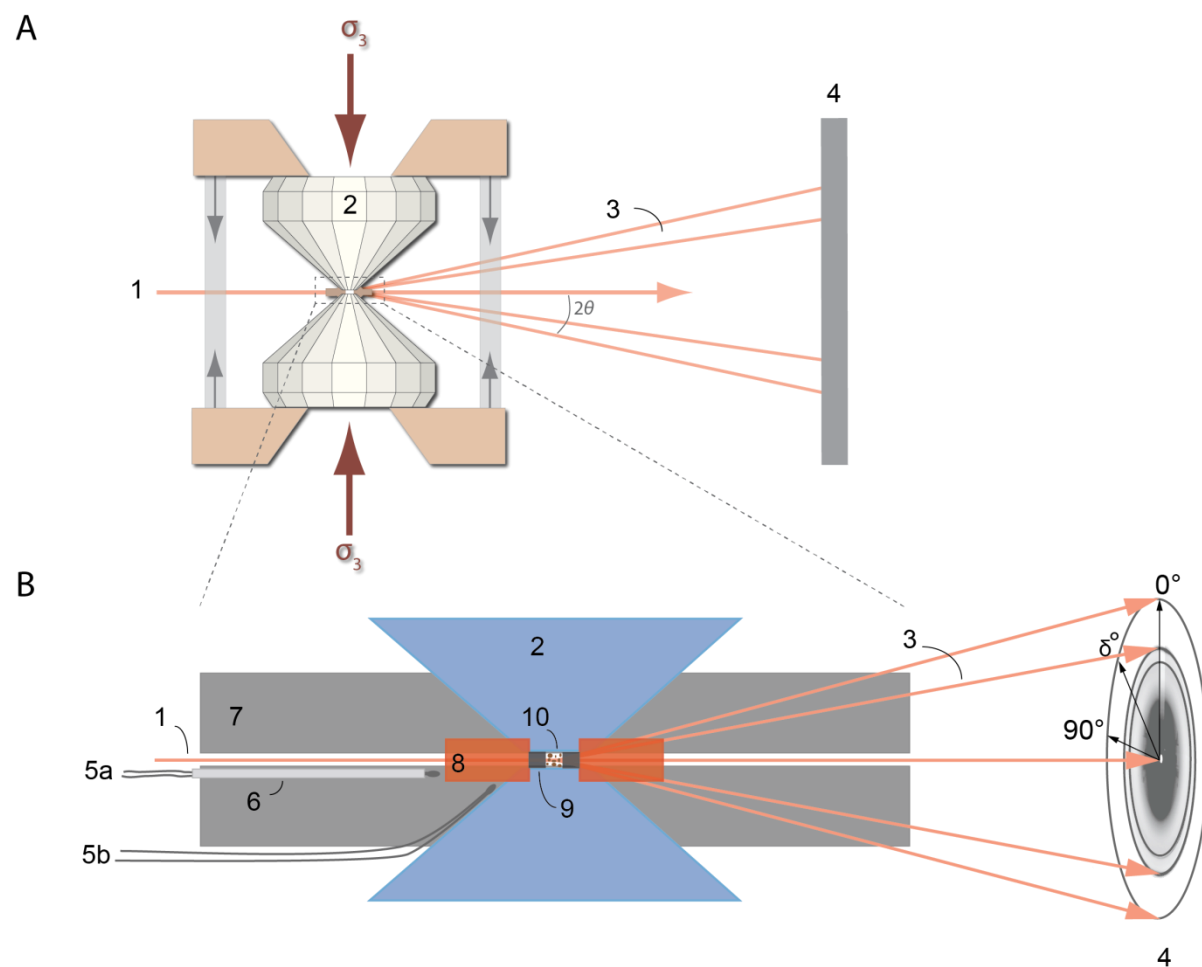
## 13 Abstract

14  
15 We present an improved setup for the experimental study of deformation of solids at  
16 simultaneous high pressures and temperatures by radial X-ray diffraction. The technique  
17 employs a graphite resistive heated Mao Bell type diamond anvil cell (DAC) for radial X-ray  
18 diffraction in combination with a water-cooled vacuum chamber. The new chamber has been  
19 developed by the sample environment group at PETRA III and implemented at the Extreme  
20 Conditions Beamline (ECB) P02.2 at PETRA III, DESY (Hamburg, Germany). We discuss  
21 applications of the new setup to study deformation of a variety of materials, including  
22 ferropericlase, calcium perovskite, bridgmanite, and tantalum carbide at high-  
23 pressure/temperature.

25 Introduction

26 Understanding the physical and rheological properties of materials at simultaneous high  
27 pressures and temperatures is of key importance in Earth science as well as materials sciences.  
28 The rheological properties of Earth's mantle materials, for example, govern large-scale mantle  
29 convection<sup>1-4</sup>. In addition, Crystallographic Preferred Orientation (CPO) caused by the  
30 alignment of mantle minerals during deformation, leads to seismic anisotropy, providing a  
31 means to link seismic observations to mantle flow<sup>5-13</sup>. Several techniques have been  
32 developed in the past to study the rheology of materials under high pressure and temperature,  
33 but achievable pressures are mostly limited to those typical of the crust and upper mantle<sup>3,14-</sup>  
34 <sup>18</sup>.

35 Deformation experiments at deep lower mantle pressures are almost exclusively performed in  
36 diamond-anvil cells in combination with synchrotron-based in-situ X-ray diffraction in a  
37 radial geometry (Fig. 1A, B). By employing radial diffraction geometry, lattice strains and  
38 deviatoric stress as well as evolution of CPO can be derived from analysis of in situ  
39 diffraction images. Radial X-ray diffraction in DACs has been widely employed in Earth as  
40 well as materials sciences, but high-pressure experiments have been mostly limited to room  
41 temperature<sup>19-25</sup>. Early high-temperature employed a laser-heated DAC, but data analysis and  
42 interpretation is challenging due to temperature gradients in the sample<sup>26,27</sup>. Liermann *et al.*,  
43 (2009)<sup>28</sup> developed a resistive-heated DAC, which was tested up to 36 GPa and 1100 K while  
44 performing in-situ radial X-ray diffraction. The use of a resistive-heating setup reduces  
45 temperature gradients and provides more homogeneous heating of the entire sample chamber.



46

47 Figure 1: (A) angle-dispersive high-pressure radial X-ray diffraction in a DAC (modified after  
48 <sup>28</sup>);  $\sigma_3$ : stress along compression direction;  $2\theta$ : diffraction angle; 1: incoming X-ray Beam; 2:  
49 Diamond anvil; 3: Diffracted beam; 4: Area detector. (B) Magnification of the diamond-anvil  
50 culets showing the position for the two thermocouples (5a: between both graphite heaters; 5b:  
51 on the diamond anvil next to the culet). 6: Ceramic sleeve; 7: Flexible graphite sheet; 8:  
52 Kapton; 9: Boron gasket; 10: sample.

53

54 Here, we present a modified resistive-heated-radial-X-ray-diffraction-diamond-anvil-cell  
55 (RH-rXRD-DAC) (Fig. 2A, B) and report on its performance during in-situ radial X-ray  
56 diffraction experiments at simultaneous high pressure and high temperature on several

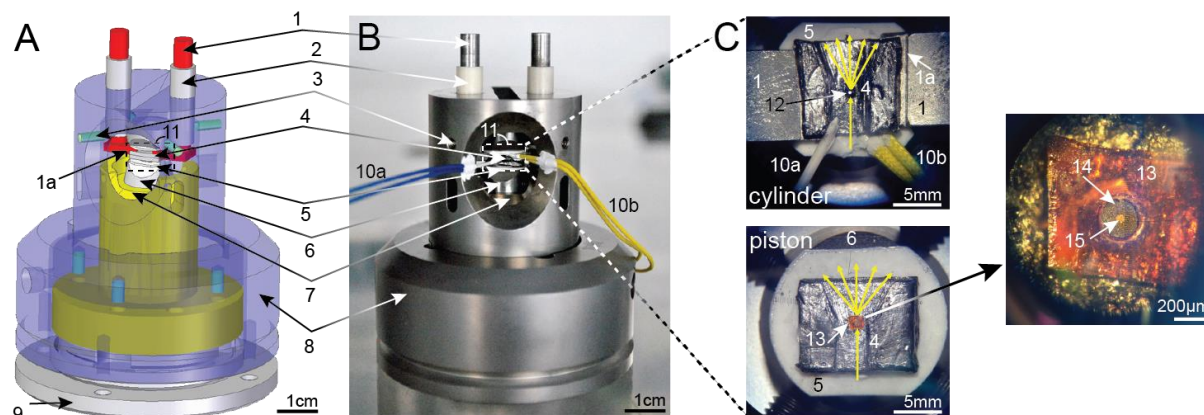
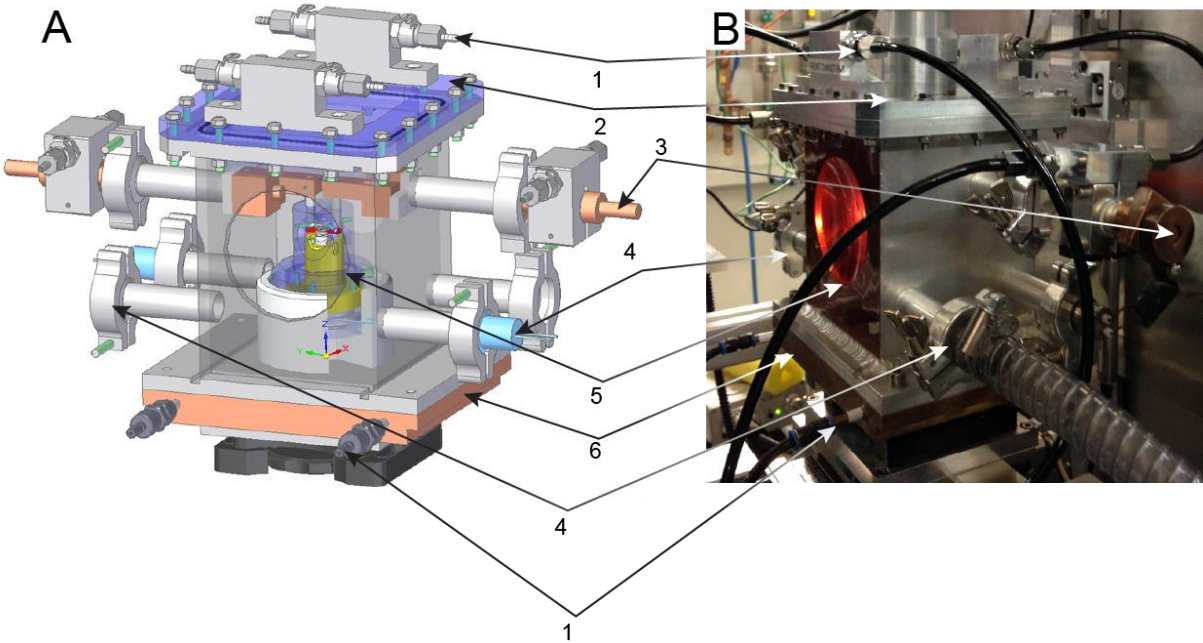


Figure 2: Experimental setup of a resistive-heated DAC (modified after<sup>10</sup>). (A) 3D CAD model and (B) photograph of the resistive-heated DAC used for the experiments. 1: Molybdenum rods (electrical contacts); 1a: Strip with step at the end of molybdenum rod; 2: Ceramic sleeves; 3: Screws; 4: Graphite sheet; 5: Ceramic plate; 6: Tungsten carbide seat; 7: Piston; 8: Cylinder; 9: Membrane cup (missing in B); 10a: Thermocouple with ceramic sleeve; 10b: Thermocouple; 11: Graphite-heater. (C) Close-up of 11. Cylinder: 12: Culet of a diamond; 4: Flexible graphite sheet with carved space for X-ray beam. Inset shows the lower diamond pressed into the graphite heater and illustrates the positions of the thermocouples. Piston: 13: Kapton, which supports a cubic boron nitride gasket or amorphous boron epoxy gasket (14) with powder sample in the sample chamber (15).

polycrystalline samples. The main improvement as compared to the setup described by Liermann et al. (2009) is the development and implementation of a water-cooled vacuum chamber (Fig. 3A, B) that also enables cooling of the piston of the Mao Bell type DAC. This modification decreases heating and thermal expansion of the piston of the Mao Bell DAC but allows the cylinder to heat up, thus reducing friction between the piston and the cylinder during compression at high temperatures. The use of a vacuum chamber prevents the oxidation of the cell, the Molybdenum rods and the diamonds at very high temperatures. We

76 discuss applications of the improved setup for studying the deformation behavior of major  
 77 materials expected in Earth’s lower mantle as well as tantalum carbide.



78  
 79 Figure 3: (A) 3D CAD model of the vacuum chamber. (B) Photograph of the vacuum  
 80 chamber while performing a high-temperature experiment (~1400 K). 1: Water cooling  
 81 inlet/outlet; 2: Lid with screws; 3: Power supply connector; 4: Vacuum pump connection; 5:  
 82 Kapton window; 6: Copper cooling plate.

### 83 84 Experimental Method

85 In radial X-ray diffraction experiments, the incoming X-ray beam is oriented perpendicular to  
 86 the compression direction, i.e. the axis of the diamond anvils (Fig. 1A, C: 1). This setup  
 87 provides the possibility to study the lattice strains, resulting from the effect of differential  
 88 stress, together with the CPO of powder samples<sup>19</sup>. A pressure-transmitting medium is not  
 89 used. This enhances the development of differential stress and texture. In order for X-rays to  
 90 reach the sample chamber in the radial diffraction geometry, X-ray transparent gaskets are  
 91 required. Here, we used either X-ray transparent amorphous boron epoxy + kapton<sup>29</sup> or cubic  
 92 boron nitride (cBN) epoxy<sup>27</sup> (10:1 Epotech 353ND) + kapton gaskets (Fig. 1: 8, 9; Fig. 2C:



13, 14) to reach high pressures<sup>30</sup>. The culet sizes of the employed diamonds were 200  $\mu\text{m}$  or 300  $\mu\text{m}$  (Fig. 2C: 12). The setup of the graphite heater is similar on the piston and cylinder side of the DAC (Fig. 2C). Diamonds are glued on tungsten carbide seats that are truncated at the side to increase the opening angle for diffracted X-rays (Fig. 2: 5). The seats are insulated from the graphite by a ceramic ring (Fig. 2: 4) fixed to the seat with OMEGABOND 500 liquid. The gaps between the ceramic plates and the diamonds are filled with ceramic glue (Resbond 989). The heads of the molybdenum rods end in horizontal strips with a small step at the end. A piece of graphite foil connects the molybdenum rods (Fig. 2A: 1a; Fig. 2B: 11; Fig. 2C: 1a) and serves as heating element surrounding the diamond-anvils. A space is carved in the graphite foil to prevent diffraction of the graphite contaminating the diffraction image. Two thermocouples (R-type) are attached to the cylinder side. One thermocouple is placed close to the tip of the diamond on the upstream side of the DAC and to the side of the path of the incident X-ray beam (Fig 2C: 10a). The second thermocouple is positioned on the graphite sheet, likewise upstream and to the side of the incident X-ray beam (Fig. 2C: 10b). When the cell is closed, the second thermocouple rests between the graphite sheets of the piston and the cylinder.

During the experiment, the temperature of the sample can be increased/decreased by varying an analog I/O signal from 0-10 V using the beamline control system. This proportionally adjusts the power of the DC power supply from 0-1800 W (0–8 V and 0–220 A)<sup>31</sup>. Pressure is changed remotely using a gas membrane device that is operated by the membrane pressure controller APD200 from Sanchez Technology<sup>27,28,32</sup>.

For high-pressure and high-temperature experiments, the RH-rXRD-DAC is placed in a newly-designed water-cooled vacuum chamber that serves to both cool the DAC and to prevent oxidation of the DAC, the molybdenum electrodes, the diamond anvils and the graphite heater (Fig. 3A, B). The piston of the DAC is indirectly cooled through a steel pin

118 that is connected to the base of the vacuum chamber, which is water-cooled. The differential  
119 cooling between the piston and the cylinder reduces the friction between the two parts of the  
120 DAC and enables a smoother pressure increase as compared to the previous experimental  
121 setup<sup>27,28</sup>. During the experiment the vacuum in the chamber can be as good as  $5 \times 10^{-3}$  mbar.  
122 Note that, due to connections between the pump and the cell chamber, vacuum levels around  
123 the diamond anvil cells may not be as efficient. Nevertheless, the achieved vacuum is  
124 sufficient to perform experiments with minimal oxidation of the heating elements.

## 125 126 Results and discussion

127 The new setup has been tested during different experimental campaigns at the ECB P02.2 at  
128 PETRA III, DESY (Hamburg, Germany). Diffraction images were collected with a XRD  
129 1621 flat panel detector from Perkin Elmer. In the following, we will describe some selected  
130 experiments in order to illustrate the capability of the new setup for Earth and materials  
131 science research. We report on the deformation of polycrystalline samples of ferropericlas  
132 ((Mg<sub>0.8</sub>Fe<sub>0.2</sub>)O), the in-situ synthesis and deformation of cubic Ca-Pv (CaSiO<sub>3</sub>), experiments  
133 performed on a two-phase mixture of bridgmanite (MgSiO<sub>3</sub>) and ferropericlas, synthesized  
134 from a mixture of enstatite glass + ferropericlas in the resistive-heated DAC, as well as the  
135 high-temperature compression of tantalum carbide (TaC<sub>0.99</sub>), an ultra-high temperature  
136 ceramic material.

### 137 138 1. *In-situ deformation of ferropericlas*

139 Ferropericlas is the second most abundant mineral in Earth's lower mantle. It may play a key  
140 role in mantle dynamics since it is rheologically weaker than bridgmanite, the dominant lower  
141 mantle phase. Furthermore, it shows a pronounced elastic anisotropy, making it one of the  
142 candidates to explain seismic shear wave polarization anisotropy in the lower mantle<sup>33</sup>.



This is the author's peer reviewed, accepted manuscript. However, the online version of record will be different from this version once it has been copyedited and typeset.

PLEASE CITE THIS ARTICLE AS DOI:10.1063/1.5143293

143 However, previous deformation studies at pressures of the lower mantle were limited to room  
144 temperature due to experimental complexity<sup>19,21–23,34,35</sup>. In Immoor *et al.* (2018), we used the  
145 described setup to measure the deformation of ferropericlase to 62 GPa at 1400 K as well as  
146 to higher pressures but lower temperature. In our 1400 K run, the pressure of the sample was  
147 increased up to 40 GPa at room temperature and afterwards heated up to 1400 K. During  
148 heating, the pressure of the sample dropped to below 20 GPa. We increased the pressure again  
149 and reached 62 GPa when diamond failure stopped the experiment. During compression, we  
150 collected high quality diffraction images of ferropericlase. Based on these results, we were  
151 able to monitor the evolution of CPO in ferropericlase and confirm a change of slip system  
152 activity at high temperature as predicted by computations<sup>10</sup>.

153

## 154 2. *In-situ synthesis and deformation of cubic CaSiO<sub>3</sub>*

155 CaSiO<sub>3</sub> perovskite is expected to be an important mineral in Earth's transition zone and lower  
156 mantle, where it is the third most abundant phase for a pyrolytic mantle composition<sup>36</sup>. In a  
157 deeply subducted oceanic slab, CaSiO<sub>3</sub> perovskite may account for up to 25 Vol.% of the  
158 transformed basaltic crust<sup>37</sup> and will affect the bulk rheological properties of the lithospheric  
159 slab. According to a recent computational study<sup>38</sup>, the shear wave anisotropy of CaSiO<sub>3</sub>  
160 perovskite is about 15-30% at conditions of the lower mantle. A strong CPO of CaSiO<sub>3</sub>  
161 perovskite may, therefore, contribute to seismic anisotropy observations, in particular in the  
162 shallow lower mantle or lowermost transition zone, where the elastic anisotropy is strongest.  
163 A previous CaSiO<sub>3</sub> perovskite study has been limited to 49 GPa at ambient conditions<sup>23</sup>. At  
164 these conditions, however, CaSiO<sub>3</sub> perovskite forms a pseudo cubic structure and the exact  
165 nature of the distortion is still under debate<sup>39–42</sup>. Whereas at temperatures typical for the lower  
166 mantle, the structure is cubic (*Pm3m*)<sup>40–43</sup> and may show a different rheological behavior.  
167 CaSiO<sub>3</sub> perovskite can be experimentally synthesized from CaSiO<sub>3</sub> wollastonite at pressures

of about 20 GPa and temperature of about 1300 K<sup>44</sup>, but is not quenchable to ambient conditions. This implies that studies of the physical properties of CaSiO<sub>3</sub> perovskite need to be performed in-situ and in the same pressure device where it has been synthesized. Using the improved RH-rXRD-DAC, we were able to synthesize CaSiO<sub>3</sub> perovskite and performed several successful deformation experiments reaching temperatures of up to 1500 K at pressures of 45 GPa (Immoor *et al.* in prep.). The starting material was amorphous CaSiO<sub>3</sub> mixed with platinum powder as pressure standard. Figure 4 shows two diffraction images collected during a compression experiment that reached a final pressure of 40 GPa at 1300 K. Cubic CaSiO<sub>3</sub> perovskite was synthesized after increasing the temperature to 1300 K at which point the pressure dropped from 33 GPa to 27 GPa as a result of the phase transition (Fig. 4B). The collected diffraction patterns show smooth diffraction rings, indicating a relatively small and homogeneous grain size of the synthesized cubic CaSiO<sub>3</sub> perovskite. The large pressure drop at the transition also caused strain heterogeneity in Pt finely mixed with the sample (see Pt peaks asymmetry in Fig. 4B).

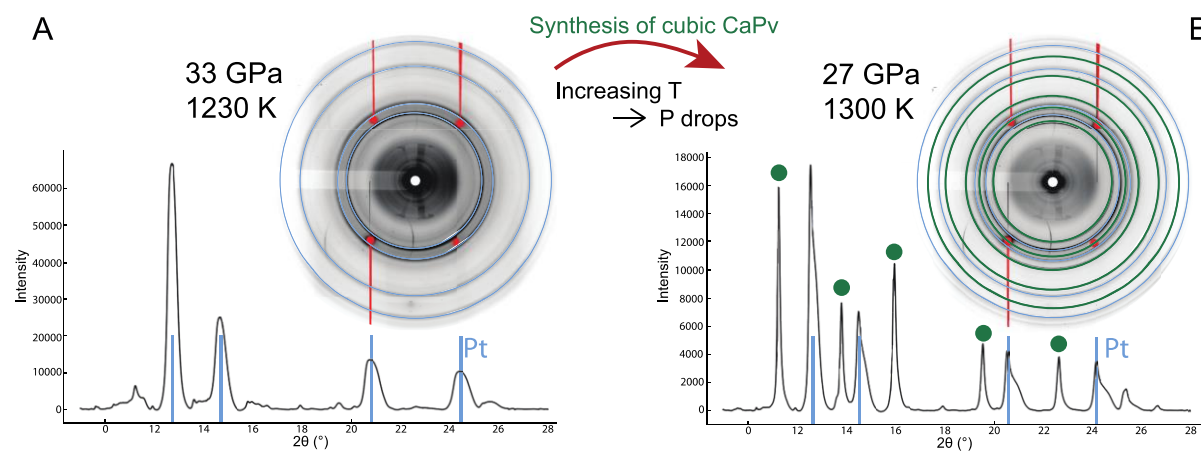


Figure 4: Synthesis of cubic calcium perovskite. The pressure was calculated from the stronger Pt peak. (A) X-ray diffraction image at 33 GPa and 1230 K shows rings of Pt (blue), which are used to estimate the pressure during the experiment and diamond single-crystal diffraction spots (red). The corresponding integrated diffraction pattern is shown below with

187 blue line indicating Pt peaks. (B) X-ray diffraction image at 27 GPa and 1300 K with Debye  
188 rings of Pt (blue), Debye rings of calcium perovskite (green) and diamond diffraction spots  
189 (red). At the bottom integrated diffraction pattern with blue lines indicating Pt peaks and  
190 green dots indicating calcium perovskite peaks.

191 In both panel (A) and (B) the diffraction lines of diamond are masked in the integration and  
192 absent in the diffraction patterns.

193

### 194 *3. Synthesis of Bridgmanite and Ferropericlas*

195 The deformation behavior of multiphase rock assemblies might substantially differ from the  
196 behavior of single-phase assemblies, particularly if the phases show large differences in  
197 rheological properties<sup>35,45–48</sup>. The lower mantle can be modeled as a two-phase mixture of  
198 bridgmanite and ferropericlas, two phases that show large differences in plastic strength and  
199 viscosity<sup>3,5,22</sup>. Because of this large contrast in rheological strength, it is difficult to predict  
200 mantle properties, including viscosity and seismic anisotropy, from single-phase  
201 measurements. There have been few deformation experiments on analogues<sup>49,50</sup>, as well as on  
202 a true two-phase lower mantle mixture at pressures and temperature of the very top of the  
203 lower mantle using a rational Drickamer apparatus<sup>3</sup>. Here, we used the improved RH-rXRD-  
204 DAC to synthesize a bridgmanite and ferropericlas assembly (Fig. 5A, B) from an enstatite  
205 glass powder mixed with ferropericlas, and applied deviatoric stress to the two-phase  
206 mixture at high temperatures (Fig. 5C). In one successful run, we first increased the pressure  
207 at 1600 K. Afterwards the pressure in the sample decreased while increasing the temperature  
208 continuously to 1900 K. A peak splitting of ferropericlas was observed, likely as a result of  
209 pressure gradients in the sample chamber, followed by the appearance of the typical  
210 diffraction ring triplet of the new phase bridgmanite. Bridgmanite grew while the pressure  
211 continued to decrease when the thermocouples stopped working. During a subsequent

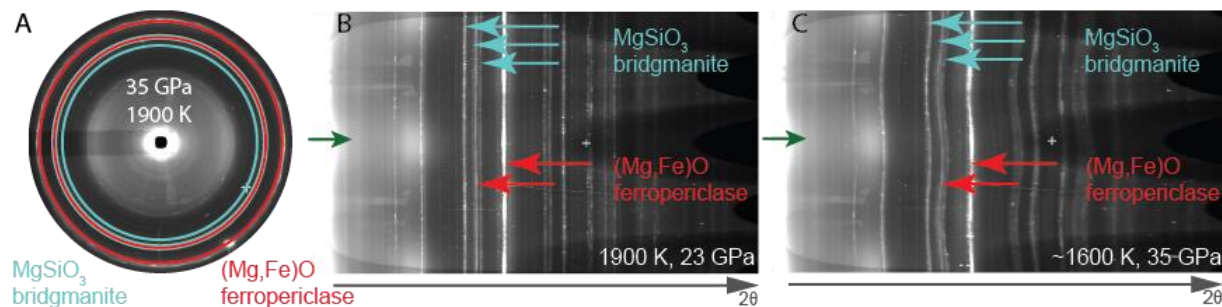


Figure 5: Synthesis of bridgmanite (blue) + ferropericase (red). Green arrows indicate the compression direction in the unrolled radial X-ray diffraction image. (A) shows the diffraction rings of bridgmanite and ferropericase at 35 GPa and 1900 K. (B) shows the unrolled image with the straight unrolled diffraction rings of bridgmanite and ferropericase at 23 GPa and 1900 K. (C) The unrolled diffraction image shows the curved unrolled diffraction rings of bridgmanite and ferropericase after pressure increase up to 35 GPa at ~1600 K. Ferropericase was used as pressure calibrant.

decrease of voltage and therefore presumably of temperature (based on power-temperature relation; see Fig. 6), the pressure in the sample chamber increased again to 35 GPa leading to deformation of the sample (Fig. 5C).

#### 4. Compression of tantalum carbide ( $TaC_{0.99}$ )

Carbides are characterized by high mechanical and thermal stability and play an important role in industrial applications, where they are used, for example, as coatings for abrasive tools. Many experimental and computational studies have been conducted on tantalum carbide (see references in<sup>51</sup>). However, no experiments have been performed to study the behavior of this phase under simultaneous high pressure, high temperature and deviatoric stress. We performed two successful experimental deformation runs on tantalum carbide ( $TaC_{0.99}$ ) and constrained the pressure-volume-temperature equation of state<sup>51</sup>. The starting material was

233 TaC<sub>0.99</sub> powder and the pressure was determined by a thin piece of Au foil (less than 5  $\mu\text{m}$ )  
234 using the EOS published in Fei et al. (2007). In the first run, we started heating when the  
235 pressure reached 2 GPa, we increased the temperature to 673 K, and measured X-ray  
236 diffraction up to a final pressure of 33 GPa along the 673 K isotherm. In the second run, we  
237 increased temperature at a pressure of  $\sim 2$  GPa up to 1073 K, and we collected X-ray  
238 diffraction images up to a final pressure of  $\sim 38$  GPa along an isothermal path. The data  
239 collected under non-hydrostatic conditions were used to constrain the quasi-hydrostatic high  
240 temperature EOS by extracting the hydrostatic unit-cell parameter from the x-ray diffraction  
241 data<sup>53</sup>. In addition these data can be used to determine the strength and activity of the slip  
242 systems of TaC<sub>0.99</sub> at simultaneous high-pressure and -temperature (Speziale *et al.* in prep.).

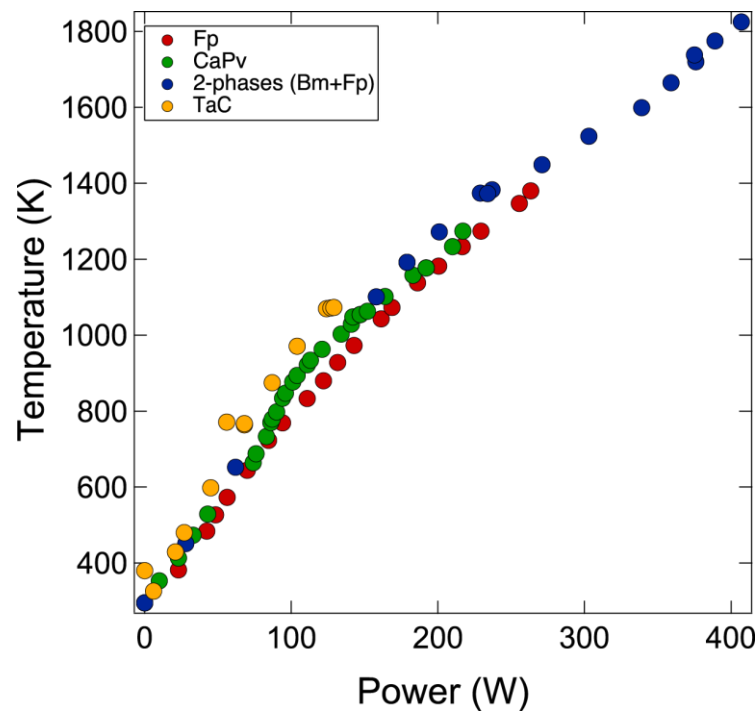
243

244 *5. Challenges and solutions*

245 In several experimental runs the DAC jammed during high-temperature experiments leading  
246 to discrete pressure jumps as opposed to smooth increases of pressure. Because of their  
247 brittleness the ceramic gaskets were not able to buffer these pressure jumps resulting in failure  
248 of the diamond anvils. The reason for our difficulties to smoothly increase pressure at very  
249 high temperatures could be the expansion of both the piston and the cylinder of the Mao Bell  
250 DAC leading to increased friction between both parts. However, at moderately high  
251 temperatures, up to 1400 K, the differential cooling was effective such that a smooth pressure  
252 increase is generally possible. For higher temperature experiments the indirect piston cooling  
253 is still insufficient, and needs to be improved in order to reduce the thermal expansion of the  
254 piston and thus the friction.

255 Using the water-cooled vacuum chamber, temperatures up to 1900 K have been reached in the  
256 RH-rXRD-DAC, but no pressure increase was possible. Generally, both thermocouples

257 recorded stable temperatures during the experiments, with a reproducible dependence of  
258 temperature on power (Fig. 6).  
259 In a few runs, the difference in temperature reading between the two thermocouples was very  
260 large (the maximum difference observed was 400 K). In these cases higher temperature values  
261 were recorded by the thermocouple situated between the graphite sheets. Large differences in  
262 temperature reading usually occurred when one of the thermocouples, i.e. the one at the tip of  
263 the diamond was placed too far from the culet of the diamond.



264  
265 Figure 6: Power – Temperature curves of different experiments. The temperature is read using  
266 two thermocouples, one placed between the two graphite heaters and one placed on the  
267 diamond-anvil close to the sample. Symbols: Fp is ferropericlase; CaPv is calcium perovskite;  
268 Bm is bridgmanite; TaC is tantalum carbide.

269

## 270 Conclusion

271 We have presented an improved experimental setup for radial X-ray diffraction measurements  
272 based on a graphite-heated Mao Bell type diamond-anvil cell contained in a water-cooled



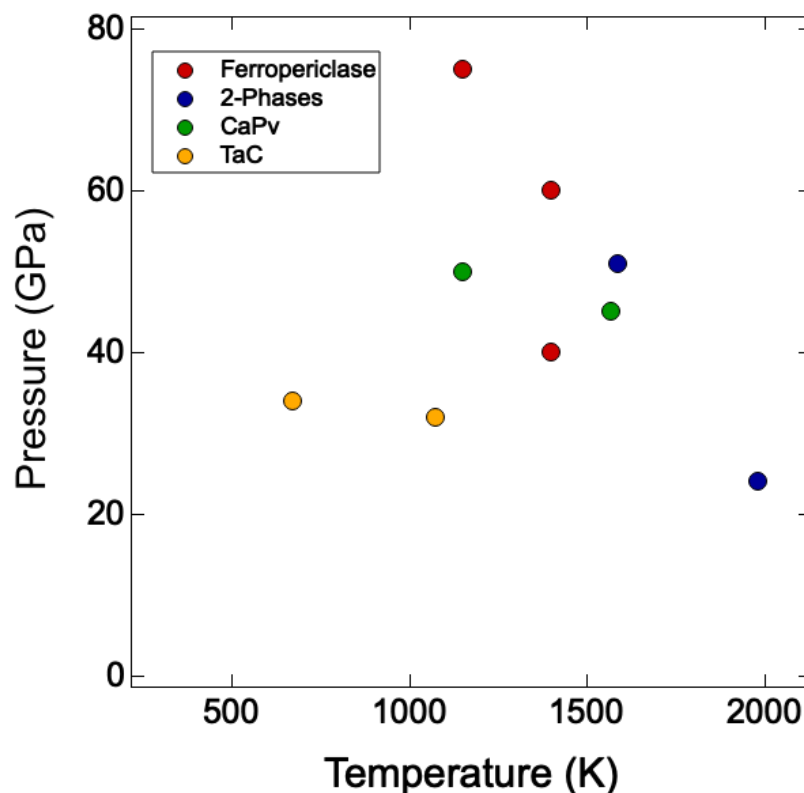


Figure 7: Maximum pressure-temperature- conditions reached in experiments on ferropericlase (red, calculated pressure), 2-phases (enstatite (bridgmanite) + ferropericlase) (blue, estimated pressure), calcium perovskite CaPv (green, 45 GPa estimated pressure; 50 GPa calculated pressure) and tantalum carbide TaC (yellow, calculated pressure) in different experimental runs.

Temperature and pressure in the diamond-anvil cell are controlled remotely during the experiment. Several successful experiments studies were performed by using the improved setup on a variety of Earth materials (ferropericlase, calcium perovskite, a two-phase bridgmanite-ferropericlase mixture) and tantalum carbide in order to show the capabilities of the resistive-heated-radial-X-ray-diffraction-diamond-anvil-cell. A major priority is currently

287 the search for a better gasket material which combines mechanical strength and high-  
288 temperature stability.

289

290 Acknowledgements

291 This research was supported through the projects “GeoMaX” funded under the Emmy-  
292 Noether Program of the German Science Foundation (MA4534/3-1) as well as grant  
293 MA4534/4-1. HM acknowledges support from the Bavarian Academy of Sciences. LM  
294 acknowledges support from the US Department of Energy, National Nuclear Security  
295 Administration, through the Capital-DOE Alliance Center (DE-NA0003858) and NSF (EAR-  
296 1344579 and EAR-1654687). SM acknowledges support from the Institut Universitaire de  
297 France and the program PNP of CNRS/INSU. We acknowledge DESY (Hamburg, Germany),  
298 a member of the Helmholtz Association HGF, for the provision of experimental facilities.  
299 Parts of this research were carried out at PETRA III and we would like to thank K. Glazyrin  
300 for assistance in using Beamline P02.2. Part of the research leading to this result has been  
301 supported by the project CALIPSO plus under the Grant Agreement 730872 from the EU  
302 Framework Programme for Research and Innovation HORIZON 2020.

303

# References

- <sup>1</sup> D.L. Kohlstedt, *Properties of Rocks and Minerals - Constitutive Equations, Rheological Behavior, and Viscosity of Rocks* (Elsevier B.V., 2007).
- <sup>2</sup> N. Tsujino, Y. Nishihara, D. Yamazaki, Y. Seto, Y. Higo, and E. Takahashi, *Nature* 539, 81 (2016).
- <sup>3</sup> J. Girard, G. Amulule, R. Farla, A. Mohiuddin, and S. Karato, *Science*. 351, 144 (2016).
- <sup>4</sup> S. Karato and P. Wu, *Science*. 260, 771 (1993).
- <sup>5</sup> D. Yamazaki and S. Karato, *Am. Mineral.* 86, 385 (2001).
- <sup>6</sup> B. Romanowicz and H.R. Wenk, *Phys. Earth Planet. Inter.* 269, 58 (2017).
- <sup>7</sup> P.J. Tackley, *Science*. 288, 2002 (2000).
- <sup>8</sup> S. Karato, *Phys. Earth Planet. Inter.* 51, 107 (1988).
- <sup>9</sup> S. Karato, S. Zhang, and H.-R. Wenk, *Science*. 270, 458 (1995).
- <sup>10</sup> J. Immoor, H. Marquardt, L. Miyagi, F. Lin, S. Speziale, S. Merkel, J. Buchen, A. Kurnosov, and H.P. Liermann, *Earth Planet. Sci. Lett.* 489, 251 (2018).
- <sup>11</sup> N. Creasy, M.D. Long, and H.A. Ford, *J. Geophys. Res. Solid Earth* 122, 5243 (2017).
- <sup>12</sup> C.P. Conrad, M.D. Behn, and P.G. Silver, *J. Geophys. Res. Solid Earth* 112, 1 (2007).
- <sup>13</sup> A. Nowacki, A.M. Walker, J. Wookey, and J.M. Kendall, *Geophys. J. Int.* 192, 1085 (2013).
- <sup>14</sup> T. Kawazoe, N. Nishiyama, Y. Nishihara, T. Irifune, D. Suetsugu, C. Bina, T. Inoue, D. Wiens, and M. Jellinek, *Phys. Earth Planet. Inter.* 183, 190 (2010).
- <sup>15</sup> Y. Wang, W.B. Durham, I.C. Getting, and D.J. Weidner, *Rev. Sci. Instrum.* 74, 3003 (2003).
- <sup>16</sup> D. Yamazaki and S.-I. Karato, *Rev. Sci. Instrum.* 72, 4207 (2001).
- <sup>17</sup> T. Kawazoe, T. Ohuchi, Y. Nishihara, N. Nishiyama, K. Fujino, and T. Irifune, *Phys. Earth Planet. Inter.* 216, 91 (2013).

- 329 <sup>18</sup> S.A. Hunt and D.P. Dobson, Rev. Sci. Instrum. 88, (2017).
- 330 <sup>19</sup> H.-R. Wenk, I. Lonardelli, S. Merkel, L. Miyagi, J. Pehl, S. Speziale, and C.E. Tommaseo,  
331 J. Phys. Condens. Matter 18, S933 (2006).
- 332 <sup>20</sup> S. Merkel, J. Phys. Condens. Matter 18, S949 (2006).
- 333 <sup>21</sup> C.E. Tommaseo, J. Devine, S. Merkel, S. Speziale, and H.R. Wenk, Phys. Chem. Miner.  
334 33, 84 (2006).
- 335 <sup>22</sup> H. Marquardt and L. Miyagi, Nat. Geosci. 8, 311 (2015).
- 336 <sup>23</sup> L. Miyagi, S. Merkel, T. Yagi, N. Sata, Y. Ohishi, and H.R. Wenk, Phys. Earth Planet.  
337 Inter. 174, 159 (2009).
- 338 <sup>24</sup> H.-R. Wenk, J.R. Baumgardner, R.A. Lebensohn, and C.N. Tomé, J. Geophys. Res. Solid  
339 Earth 105, 5663 (2000).
- 340 <sup>25</sup> S. Merkel, A.K. McNamara, A. Kubo, S. Speziale, L. Miyagi, Y. Meng, T.S. Duffy, and  
341 H.R. Wenk, Science. 316, 1729 (2007).
- 342 <sup>26</sup> M. Kunz, W. a Caldwell, L. Miyagi, and H.-R. Wenk, Rev. Sci. Instrum. 78, 063907  
343 (2007).
- 344 <sup>27</sup> L. Miyagi, W. Kanitpanyacharoen, S.V. Raju, P. Kaercher, J. Knight, A. MacDowell, H.R.  
345 Wenk, Q. Williams, and E.Z. Alarcon, Rev. Sci. Instrum. 84, 025118 (2013).
- 346 <sup>28</sup> H.-P. Liermann, S. Merkel, L. Miyagi, H.-R. Wenk, G. Shen, H. Cynn, and W.J. Evans,  
347 Rev. Sci. Instrum. 80, 104501 (2009).
- 348 <sup>29</sup> S. Merkel and T. Yagi, Rev. Sci. Instrum. 76, 2005 (2005).
- 349 <sup>30</sup> N. Funamori and T. Sato, Rev. Sci. Instrum. 79, 1 (2008).
- 350 <sup>31</sup> H.P. Liermann, Z. Konôpková, W. Morgenroth, K. Glazyrin, J. Bednarčík, E.E. McBride,  
351 S. Petitgirard, J.T. Delitz, M. Wendt, Y. Bican, A. Ehnes, I. Schwark, A. Rothkirch, M.  
352 Tischer, J. Heuer, H. Schulte-Schrepping, T. Kracht, and H. Franz, J. Synchrotron Radiat. 22,  
353 908 (2015).

- 354 <sup>32</sup> S. Merkel, H.-P. Liermann, L. Miyagi, and H.-R. Wenk, *Acta Mater.* 61, 5144 (2013).
- 355 <sup>33</sup> H. Marquardt, S. Speziale, H.J. Reichmann, D.J. Frost, F.R. Schilling, and E.J. Garnero,  
356 *Science*. 324, 224 (2009).
- 357 <sup>34</sup> J.-F. Lin, H.-R. Wenk, M. Voltolini, S. Speziale, J. Shu, and T.S. Duffy, *Phys. Chem.*  
358 *Miner.* 36, 585 (2009).
- 359 <sup>35</sup> S. Merkel, *J. Geophys. Res.* 107, (2002).
- 360 <sup>36</sup> D. Frost, *Elements* 4, 171 (2008).
- 361 <sup>37</sup> T. Irifune and T. Tsuchiya, in *Treatise Geophys. Second Ed.* (2015).
- 362 <sup>38</sup> K. Kawai and T. Tsuchiya, *Geophys. Res. Lett.* 42, 2718 (2015).
- 363 <sup>39</sup> S.-H. Shim, R. Jeanloz, and T.S. Duffy, *Geophys. Res. Lett.* 29, 2166 (2002).
- 364 <sup>40</sup> R. Caracas, R. Wentzcovitch, G.D. Price, and J. Brodholt, *Geophys. Res. Lett.* 32, 1 (2005).
- 365 <sup>41</sup> D.Y. Jung and A.R. Oganov, *Phys. Chem. Miner.* 32, 146 (2005).
- 366 <sup>42</sup> D.J. Adams and A.R. Oganov, *Phys. Rev. B - Condens. Matter Mater. Phys.* 73, 1 (2006).
- 367 <sup>43</sup> T. Komabayashi, K. Hirose, N. Sata, Y. Ohishi, and L.S. Dubrovinsky, *Earth Planet. Sci.*  
368 *Lett.* 260, 564 (2007).
- 369 <sup>44</sup> T. Uchida, Y. Wang, N. Nishiyama, K. ichi Funakoshi, H. Kaneko, A. Nozawa, R.B. Von  
370 Dreele, M.L. Rivers, S.R. Sutton, A. Yamada, T. Kunimoto, T. Irifune, T. Inoue, and B. Li,  
371 *Earth Planet. Sci. Lett.* 282, 268 (2009).
- 372 <sup>45</sup> M.R. Handy, *J. Struct. Geol.* 16, 287 (1994).
- 373 <sup>46</sup> S. Karato, *Phys. Earth Planet. Inter.* 24, 1 (1981).
- 374 <sup>47</sup> Y.-T. Takeda, *J. Struct. Geol.* 20, 1569 (1998).
- 375 <sup>48</sup> M. Thielmann, G.J. Golabek, and H. Marquardt, *Geochemistry, Geophys. Geosystems* 21, 1  
376 (2020).
- 377 <sup>49</sup> Y. Wang, N. Hilairret, N. Nishiyama, N. Yahata, T. Tsuchiya, G. Morard, and G. Fiquet,  
378 *Geochemistry, Geophys. Geosystems* 14, 3389 (2013).

This is the author's peer reviewed, accepted manuscript. However, the online version of record will be different from this version once it has been copyedited and typeset.

PLEASE CITE THIS ARTICLE AS DOI:10.1063/1.5143293

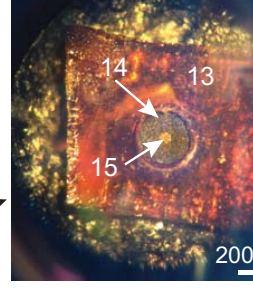
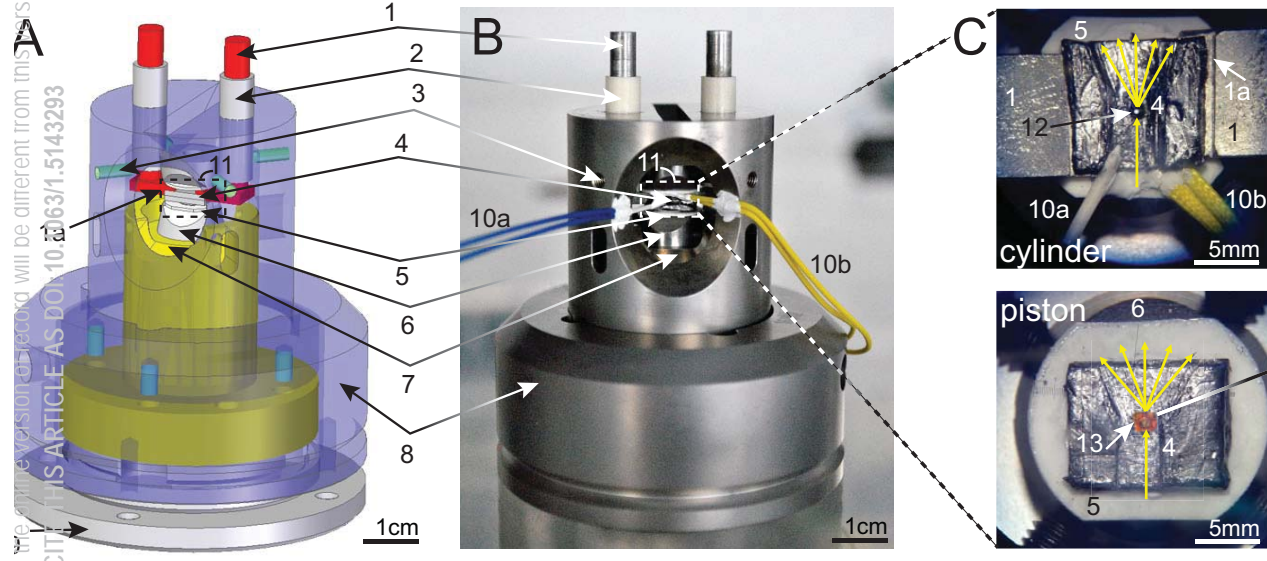
- 379 <sup>50</sup> P. Kaercher, L. Miyagi, W. Kanitpanyacharoen, E. Zepeda-Alarcon, Y. Wang, F. De Carlo,  
380 and H.-R. Wenk, Earth Planet. Sci. Lett. 456, 134 (2016).
- 381 <sup>51</sup> S. Speziale, J. Immoor, A. Ermakov, S. Merkel, H. Marquardt, and H.-P. Liermann, J.  
382 Appl. Phys. 126, 105107 (2019).
- 383 <sup>52</sup> Y. Fei, A. Ricolleau, M. Frank, K. Mibe, G. Shen, and V. Prakapenka, Proc. Natl. Acad.  
384 Sci. 104, 9182 (2007).
- 385 <sup>53</sup> S. Speziale, J. Immoor, A. Ermakov, S. Merkel, H. Marquardt, and H.-P. Liermann, J.  
386 Appl. Phys. 126, 105107 (2019).





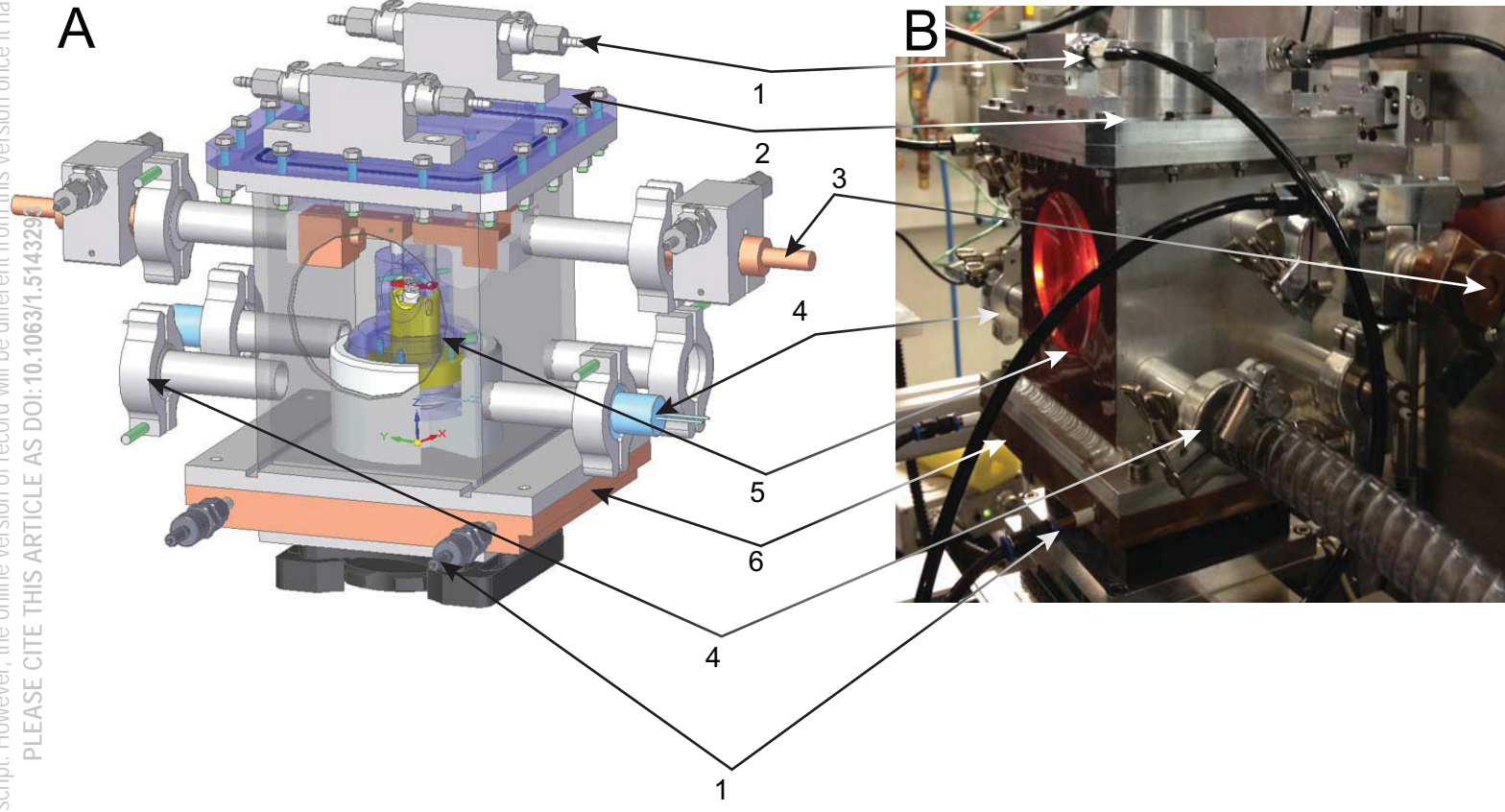
This is the author's peer reviewed, accepted manuscript. However, the copyright and/or moral rights may be reserved by the publisher. This version of the manuscript will be different from the final version once it has been copyedited and typeset.

PLEASE CITE THIS ARTICLE AS DOI:10.1063/1.5143293



This is the author's peer reviewed, accepted manuscript. However, the online version of record will be different from this version once it has been copyedited and typeset.

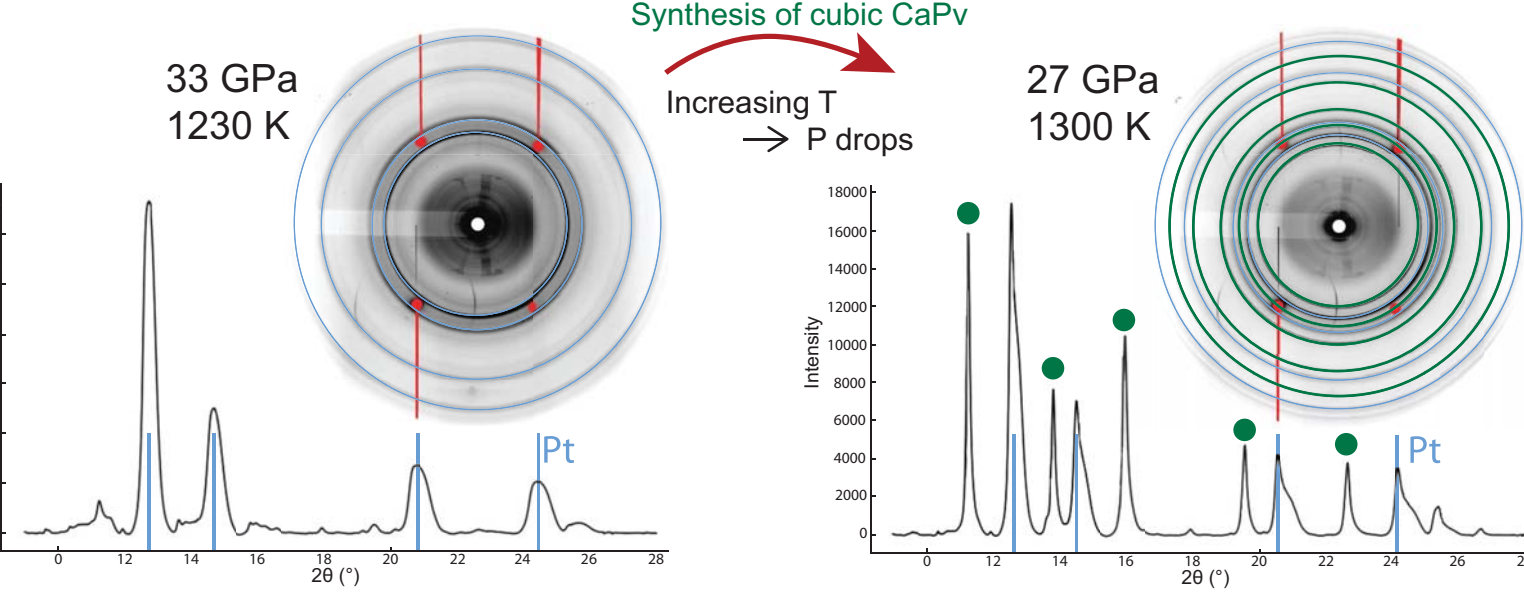
PLEASE CITE THIS ARTICLE AS DOI:10.1063/1.5143295



This is the author's peer reviewed, accepted manuscript. However, the online version of this article will be different from this version once it has been copyedited and typeset.

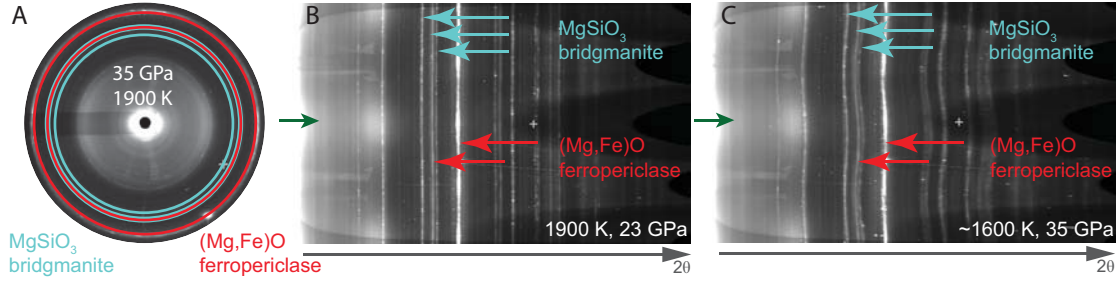
PLEASE CITE THIS ARTICLE AS DOI:10.1063/1.5143293

A



This is the author's peer reviewed, accepted manuscript. However, the online version of record will be different from this version once it has been copyedited and typeset.

PLEASE CITE THIS ARTICLE AS DOI:10.1063/1.5143293



This is the author's peer reviewed, accepted manuscript. However, the online version of record will be different from this version once it has been copyedited and typeset.

PLEASE CITE THIS ARTICLE AS DOI:10.1063/1.5143293

